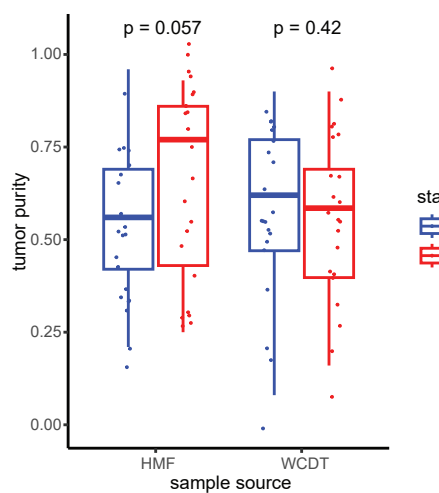
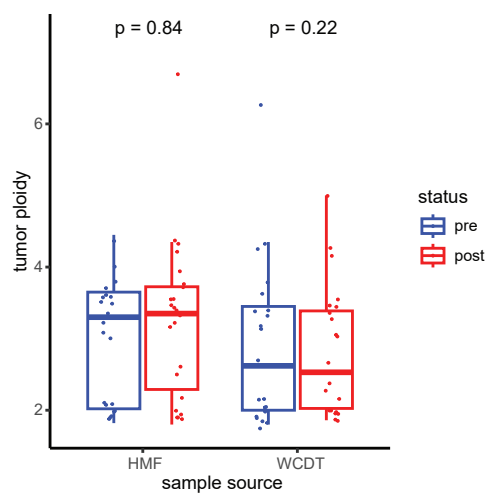
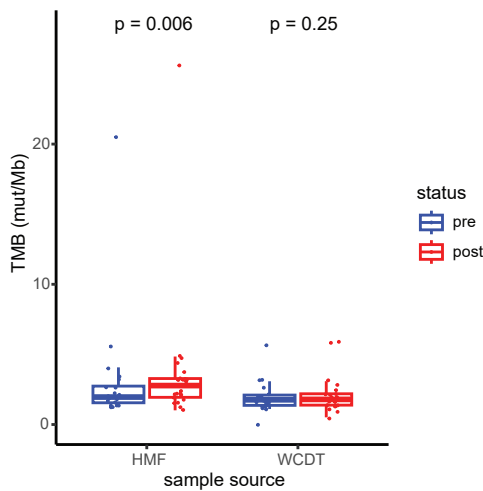
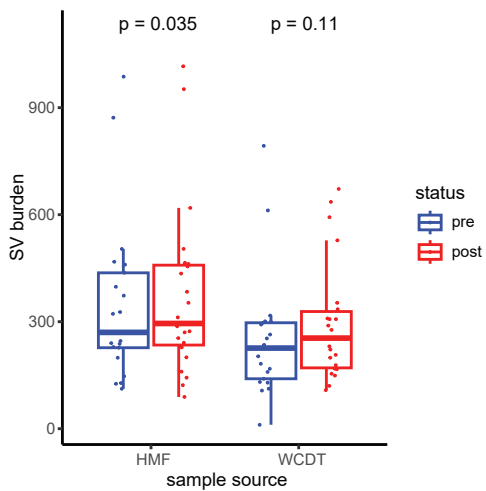
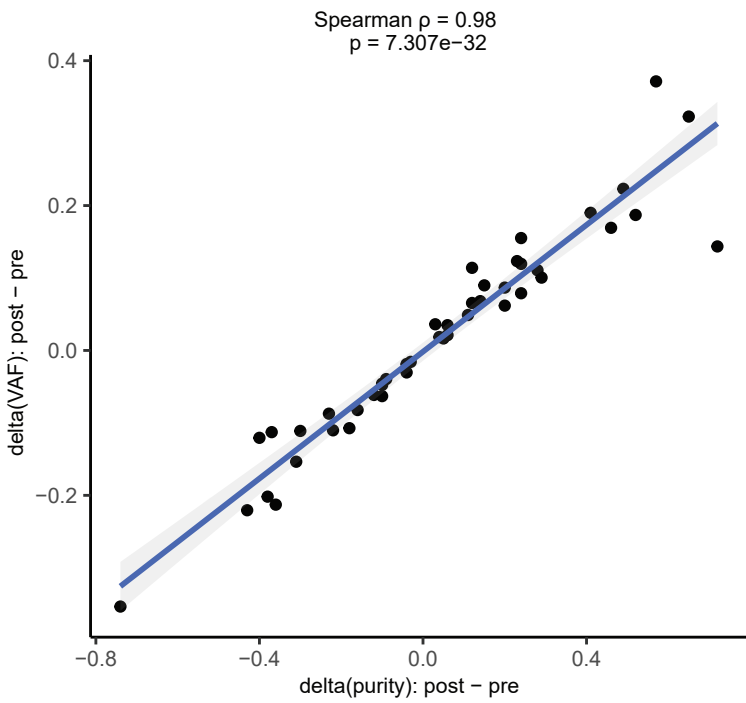
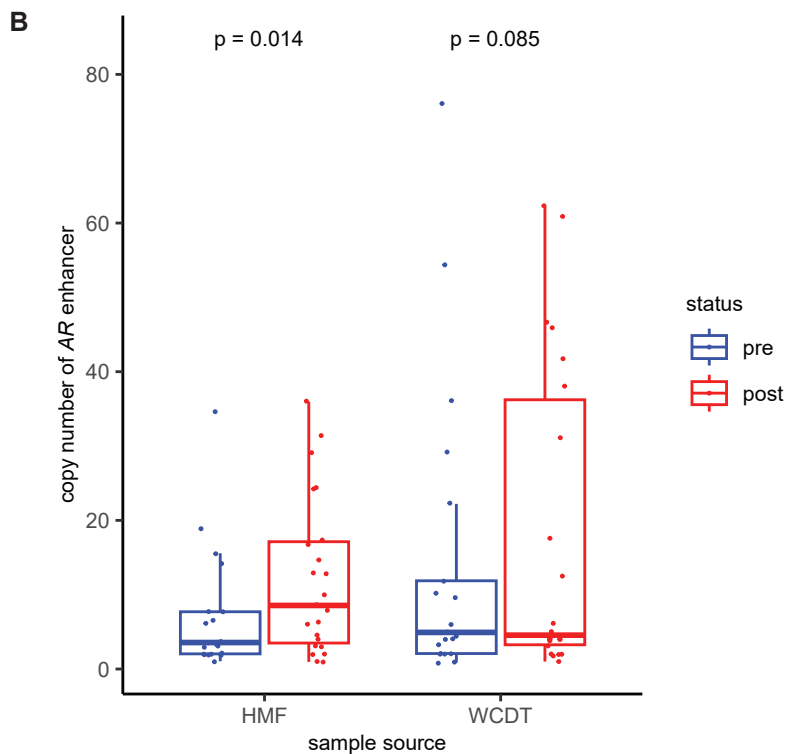
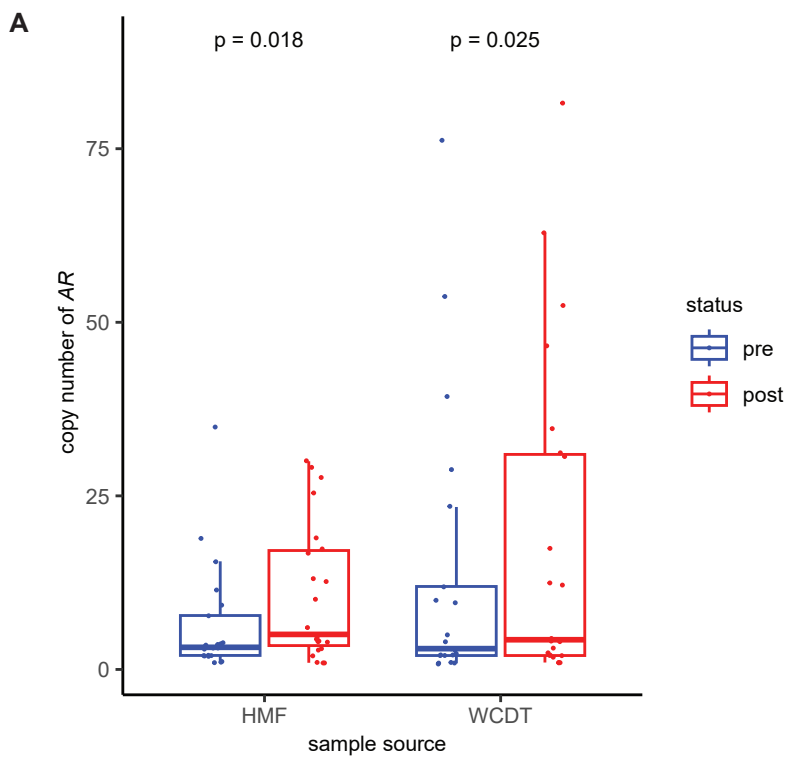
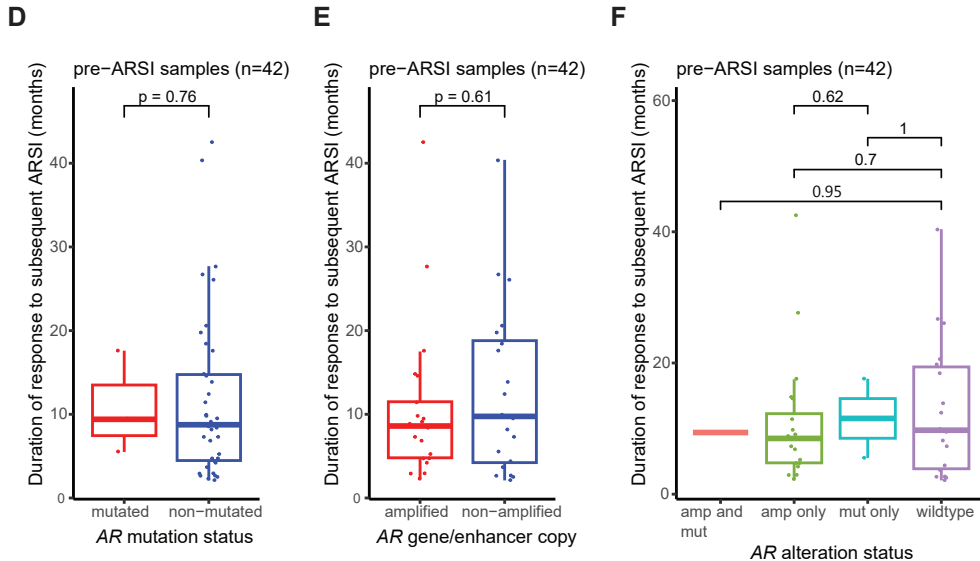
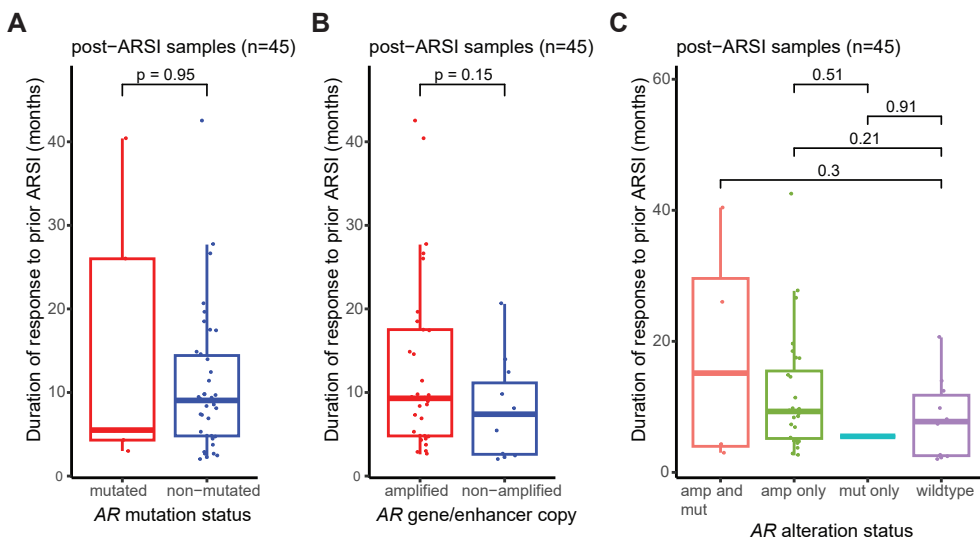
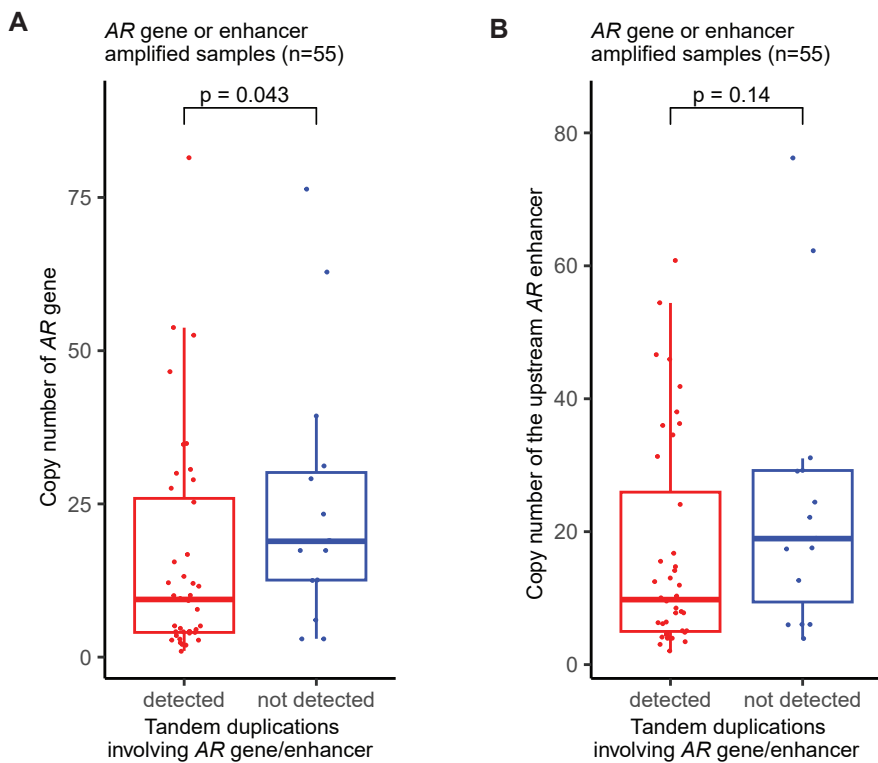


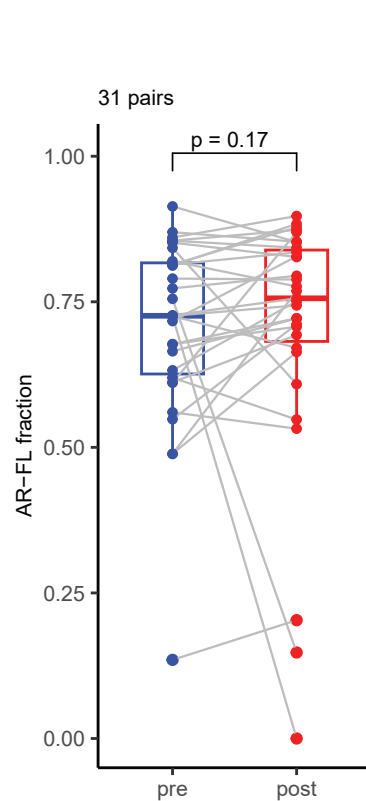
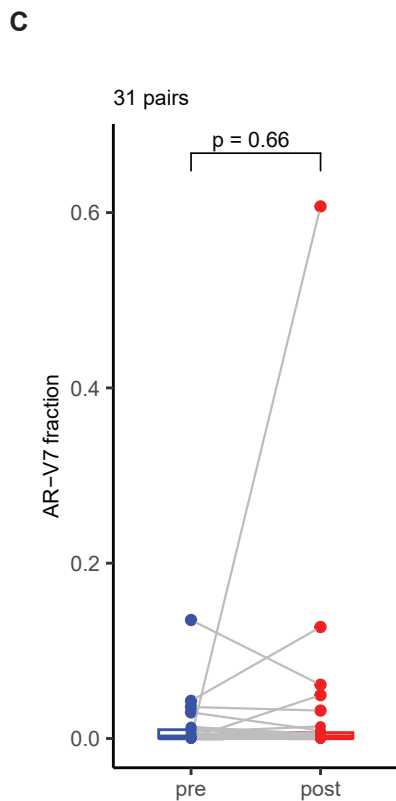
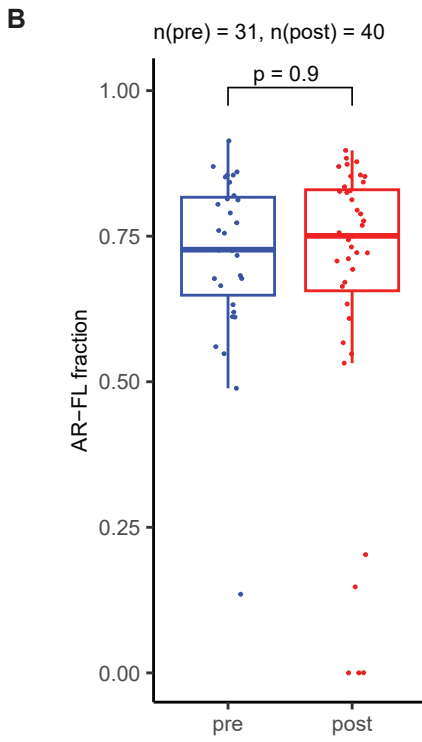
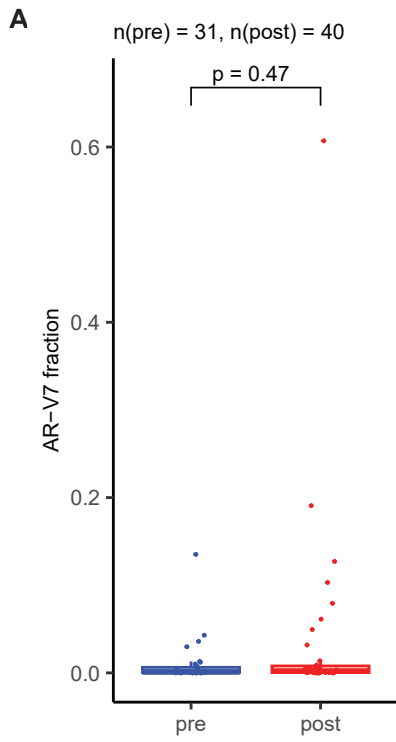
**A****B****C****D**

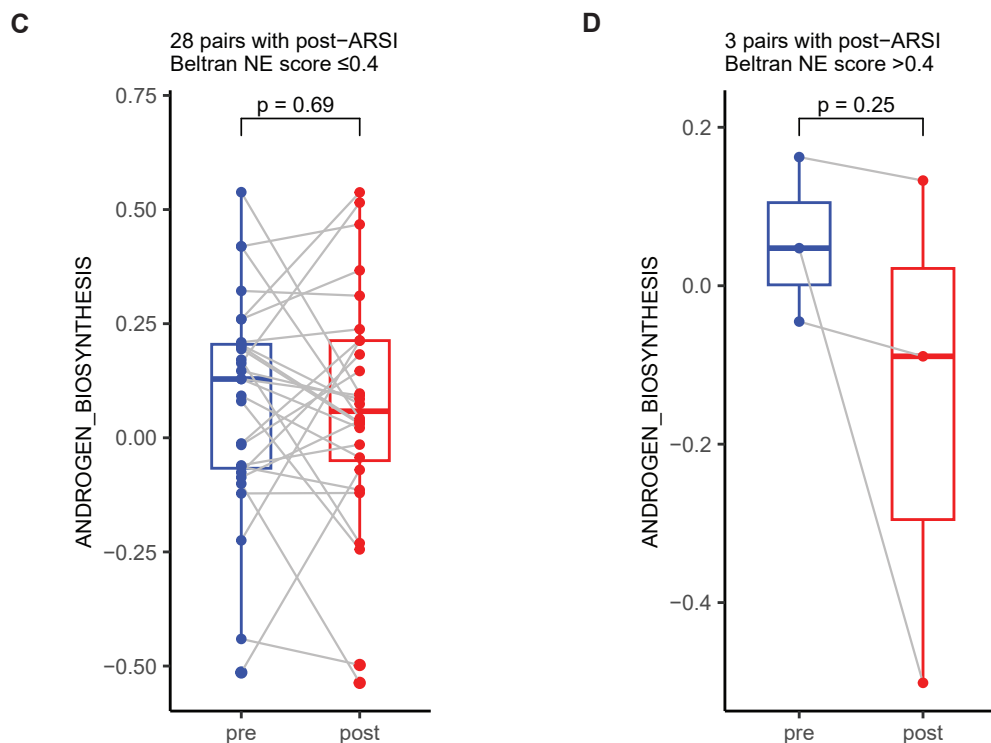
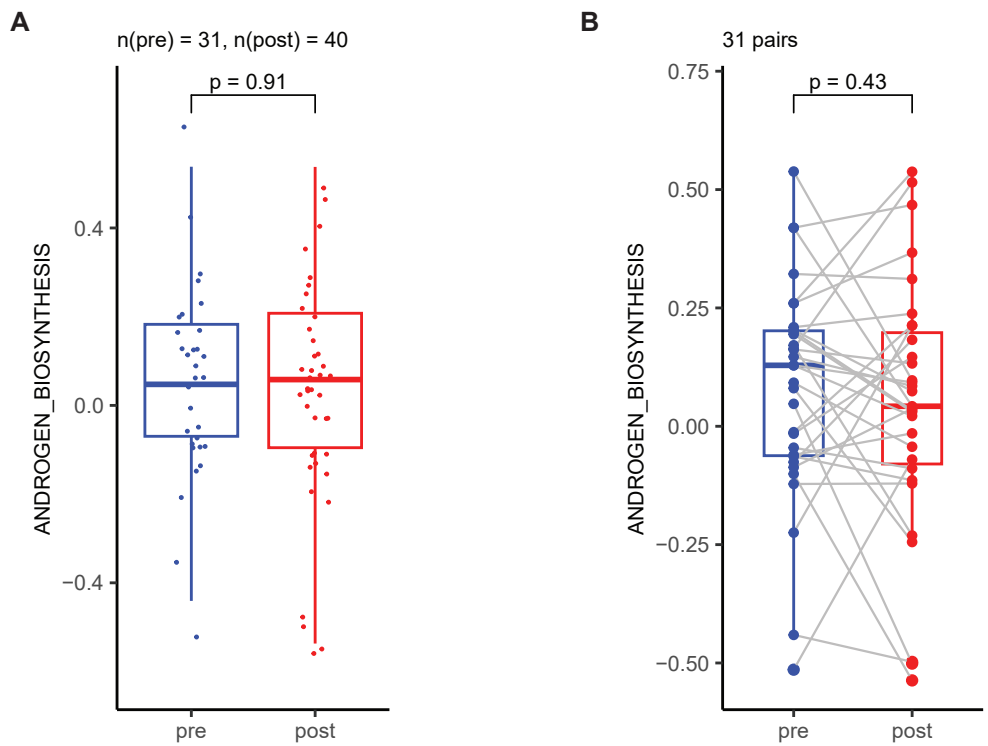


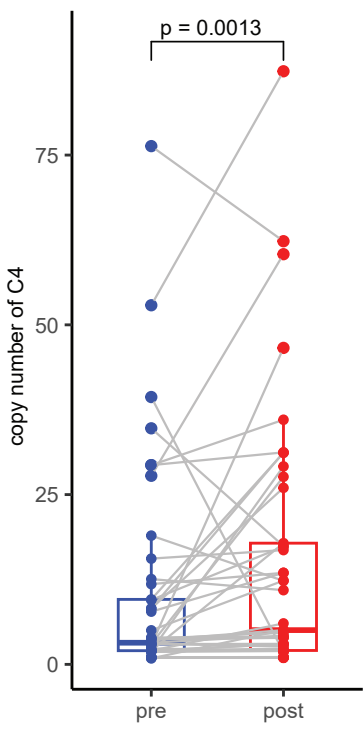


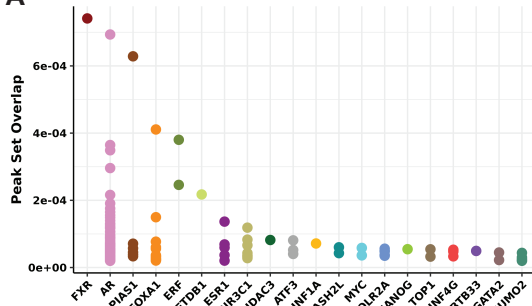
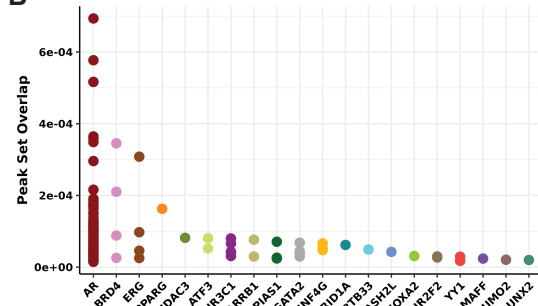
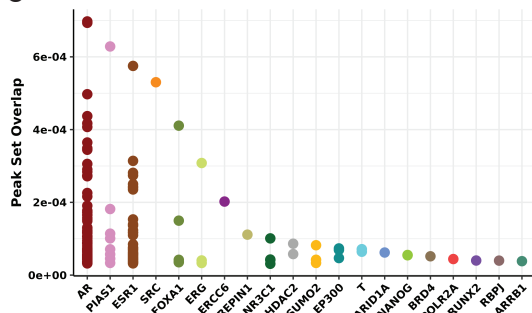
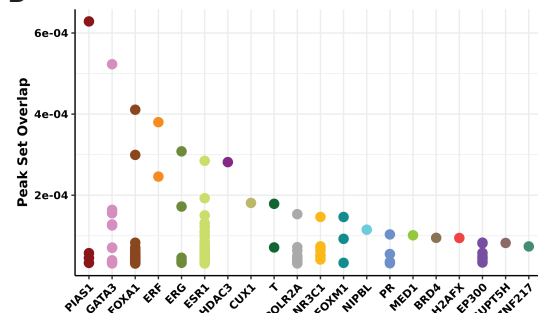


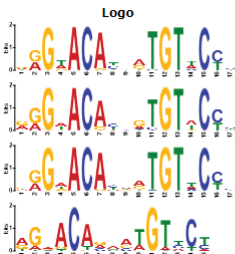




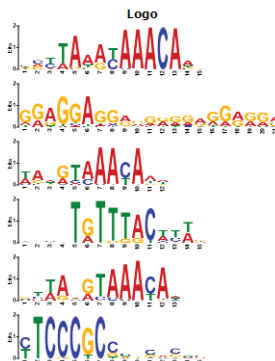




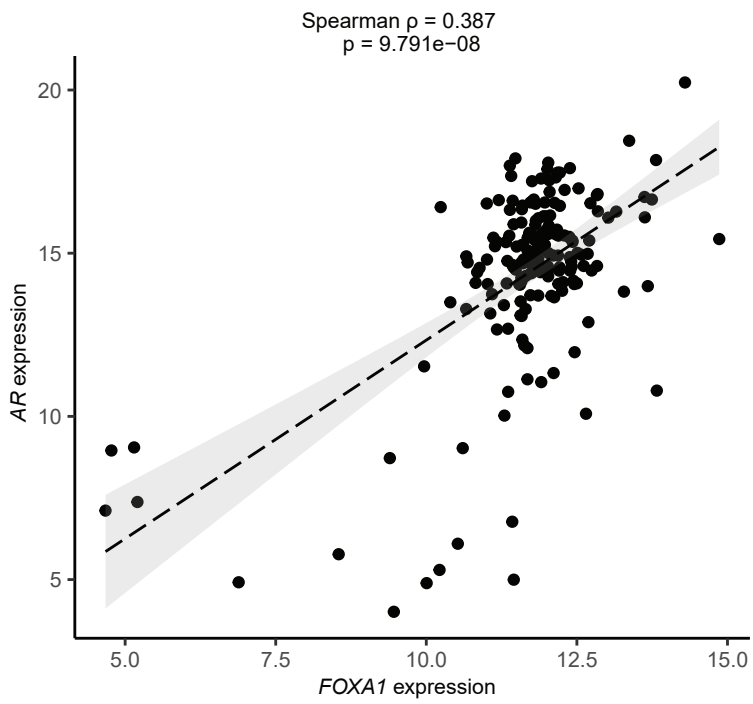
**A****B****C****D**

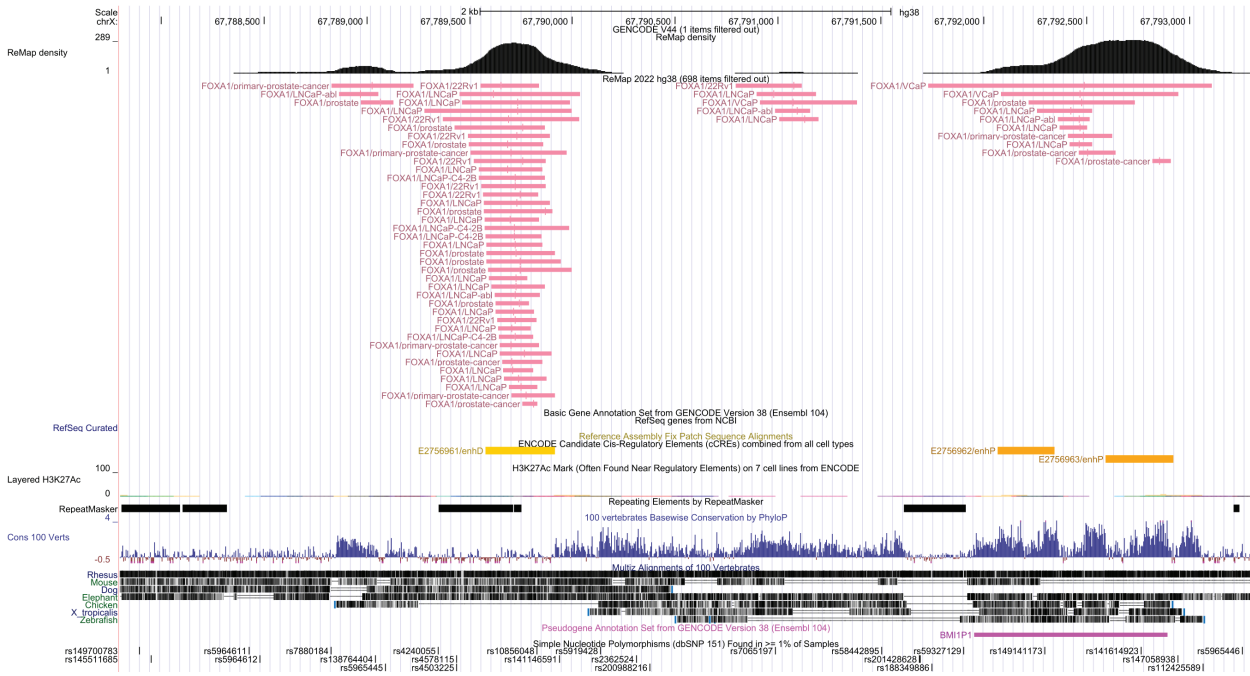
**A**

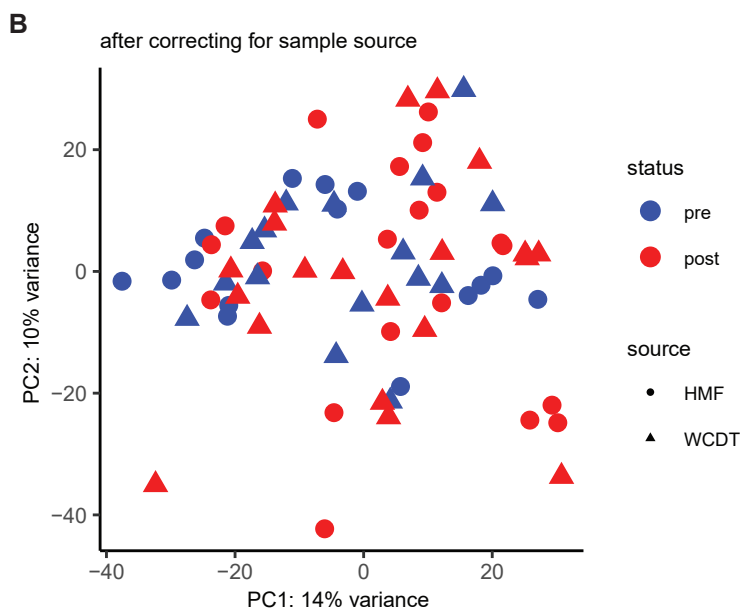
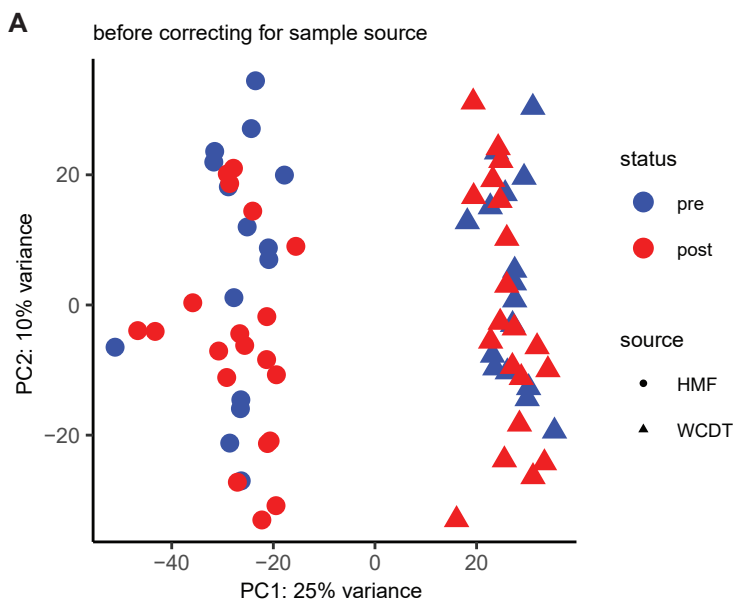
Database	ID	Alt ID	p-value	E-value	TP Thresh	TP (%)	FP (%)
JASPAR2022 CORE vertebrates redundant v2	<a href="#">MA0113.3</a>	NR3C1	6.06e-4	7.30e-1	66.22	2 (66.7%)	2 (0.2%)
JASPAR2022 CORE vertebrates redundant v2	<a href="#">MA0007.3</a>	Ar	6.77e-4	8.16e-1	66.82	2 (66.7%)	2 (0.2%)
JASPAR2022 CORE vertebrates redundant v2	<a href="#">MA0727.1</a>	NR3C2	1.19e-3	1.43e0	51.11	2 (66.7%)	3 (0.3%)
JASPAR2022 CORE vertebrates redundant v2	<a href="#">MA0113.2</a>	NR3C1	7.60e-3	9.15e0	134.31	2 (66.7%)	2 (0.2%)

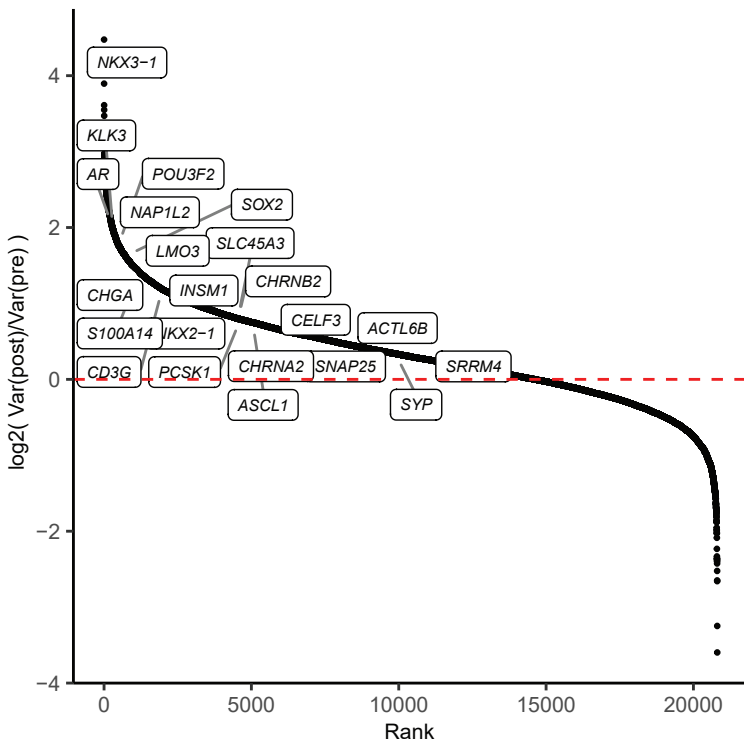
**B**

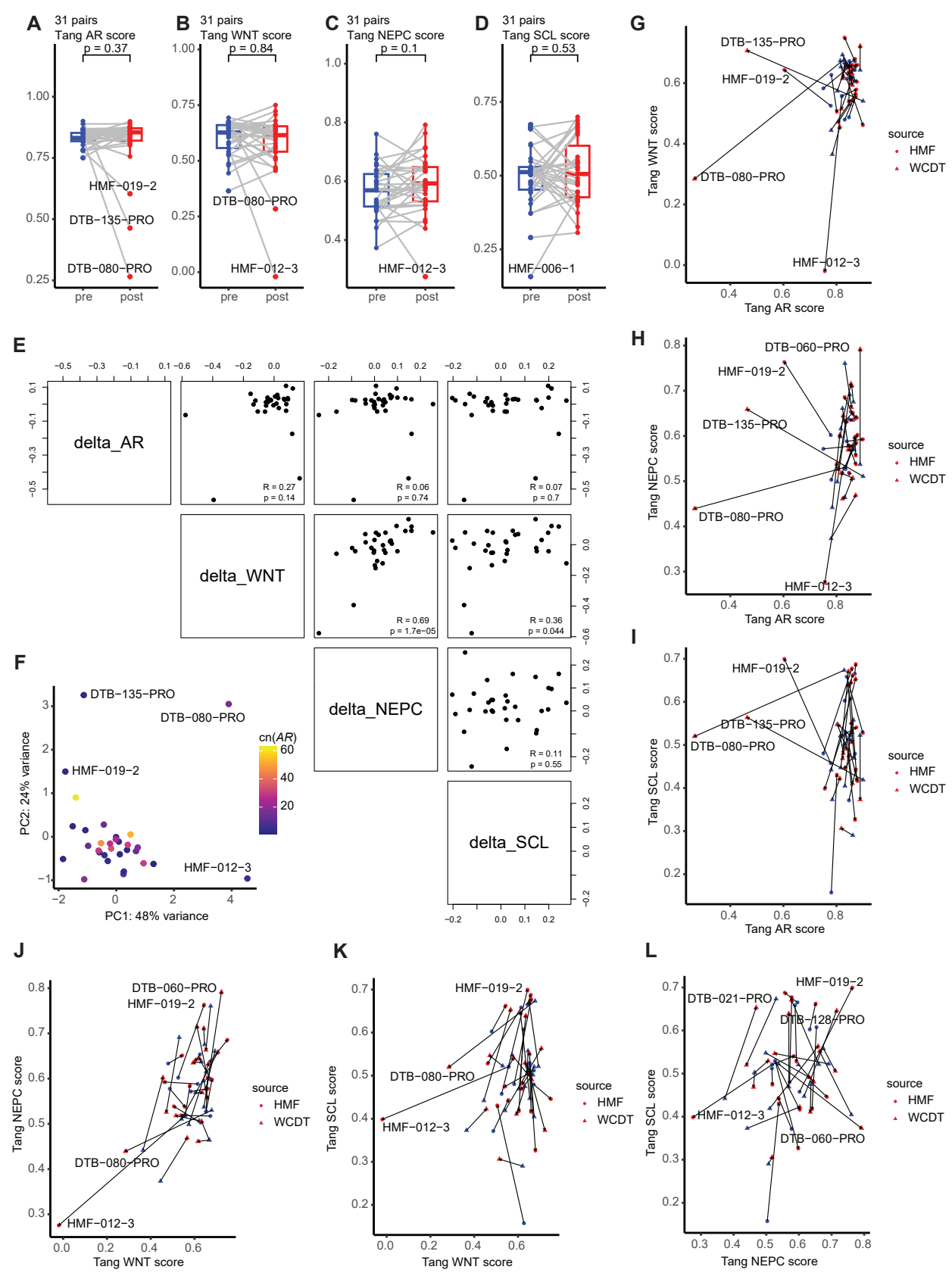
Database	ID	Alt ID	p-value	E-value	TP Thresh	TP (%)	FP (%)
JASPAR2022 CORE vertebrates redundant v2	<a href="#">MA1487.1</a>	FOXE1	2.77e-4	3.34e-1	1.45	4 (100.0%)	45 (4.5%)
JASPAR2022 CORE vertebrates redundant v2	<a href="#">MA0528.1</a>	ZNF263	9.72e-4	1.17e0	4.56	4 (100.0%)	49 (4.9%)
JASPAR2022 CORE vertebrates redundant v2	<a href="#">MA0846.1</a>	FOXC2	1.43e-3	1.73e0	3.45	4 (100.0%)	50 (5.0%)
JASPAR2022 CORE vertebrates redundant v2	<a href="#">MA0148.3</a>	FOXA1	1.59e-3	1.91e0	4.49	4 (100.0%)	53 (5.3%)
JASPAR2022 CORE vertebrates redundant v2	<a href="#">MA0847.2</a>	FOXD2	1.94e-3	2.33e0	1.99	4 (100.0%)	62 (6.2%)
JASPAR2022 CORE vertebrates redundant v2	<a href="#">MA0469.1</a>	E2F3	5.66e-3	6.82e0	8.16	2 (50.0%)	5 (0.5%)

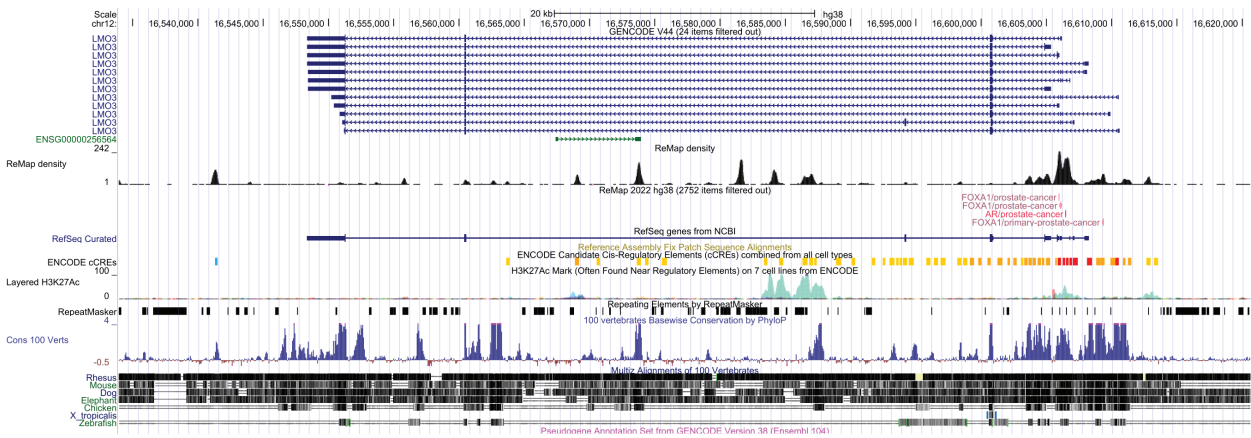


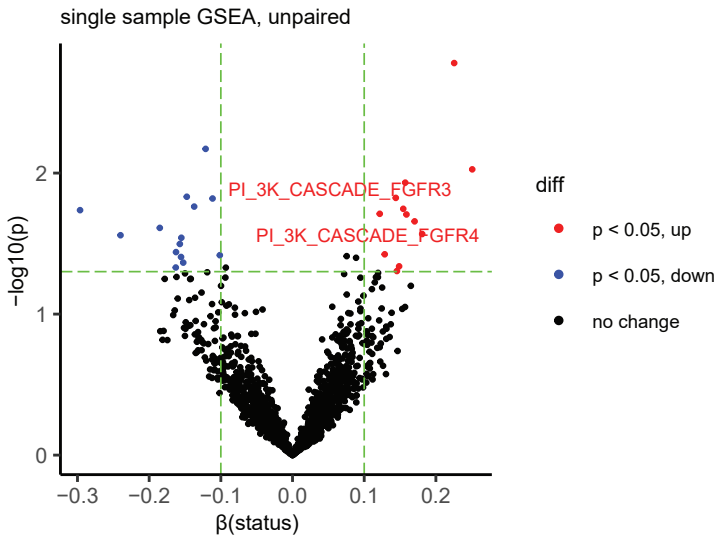




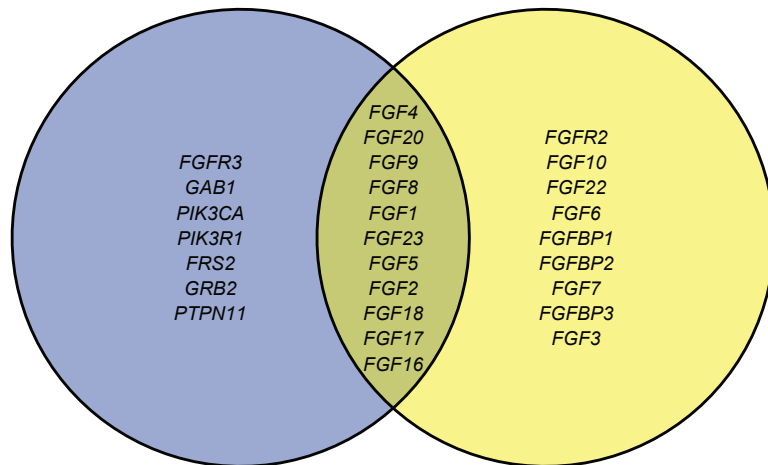


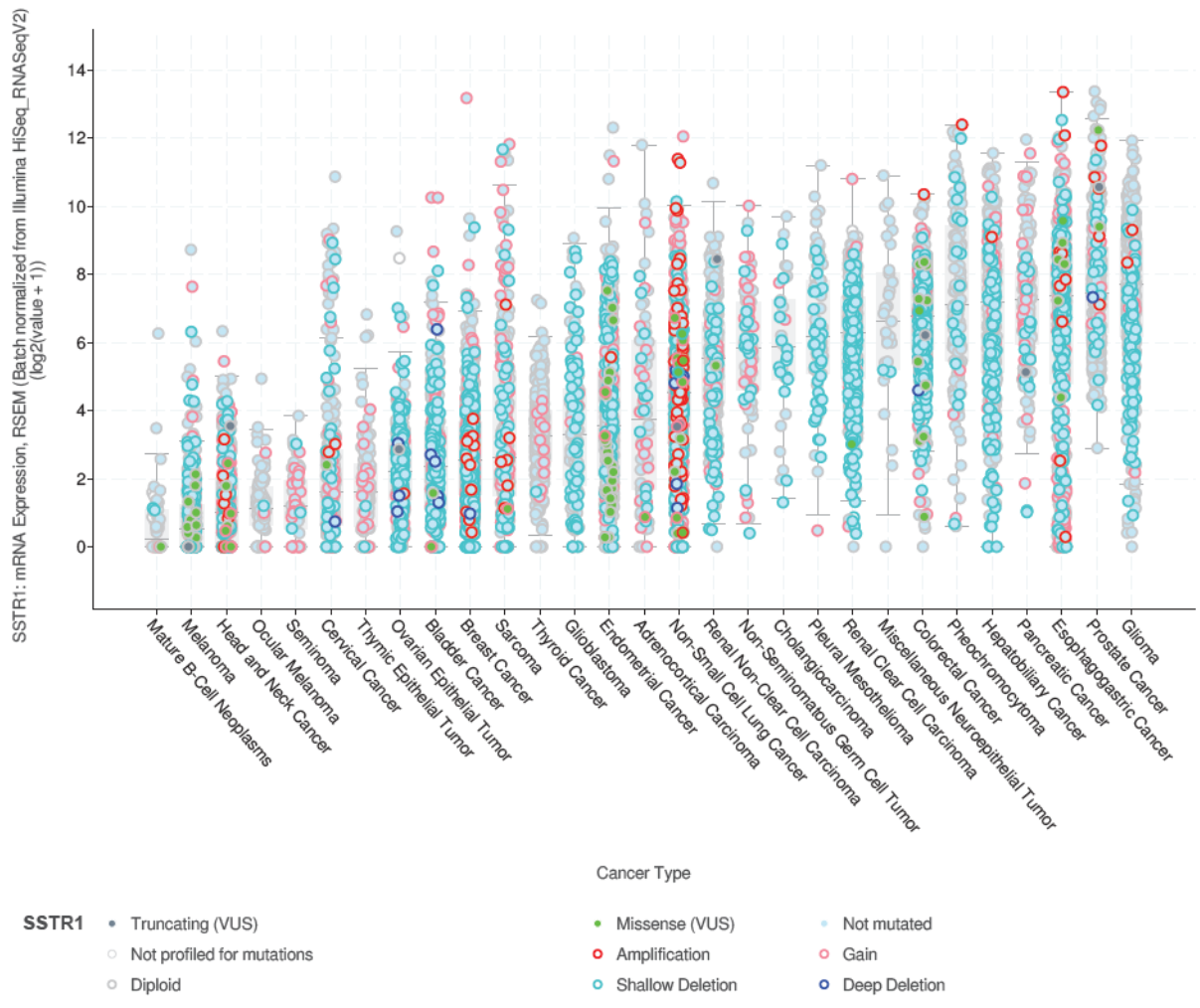




**A****B**

REACTOME\_PI\_3K CASCADE FGFR3      REACTOME\_FGFR2\_LIGAND\_BINDING\_AND\_ACTIVATION





**SSTR1** • Truncating (VUS)

○ Not profiled for mutations

○ Diploid

○ Not profiled for CNA and Structural Variants

● Missense (VUS)

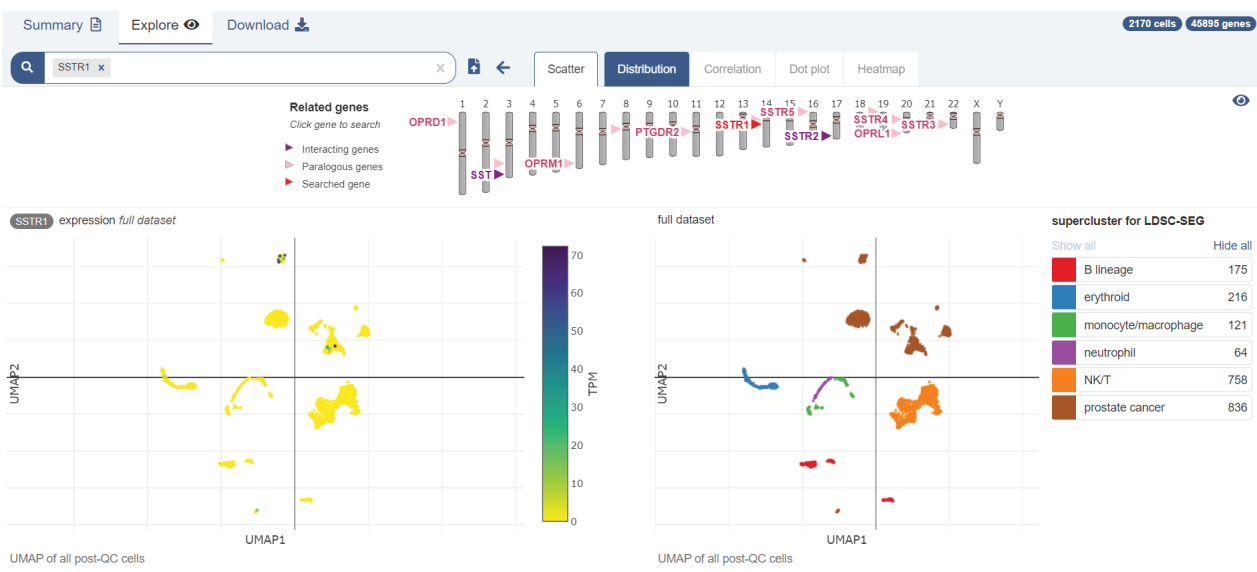
● Amplification

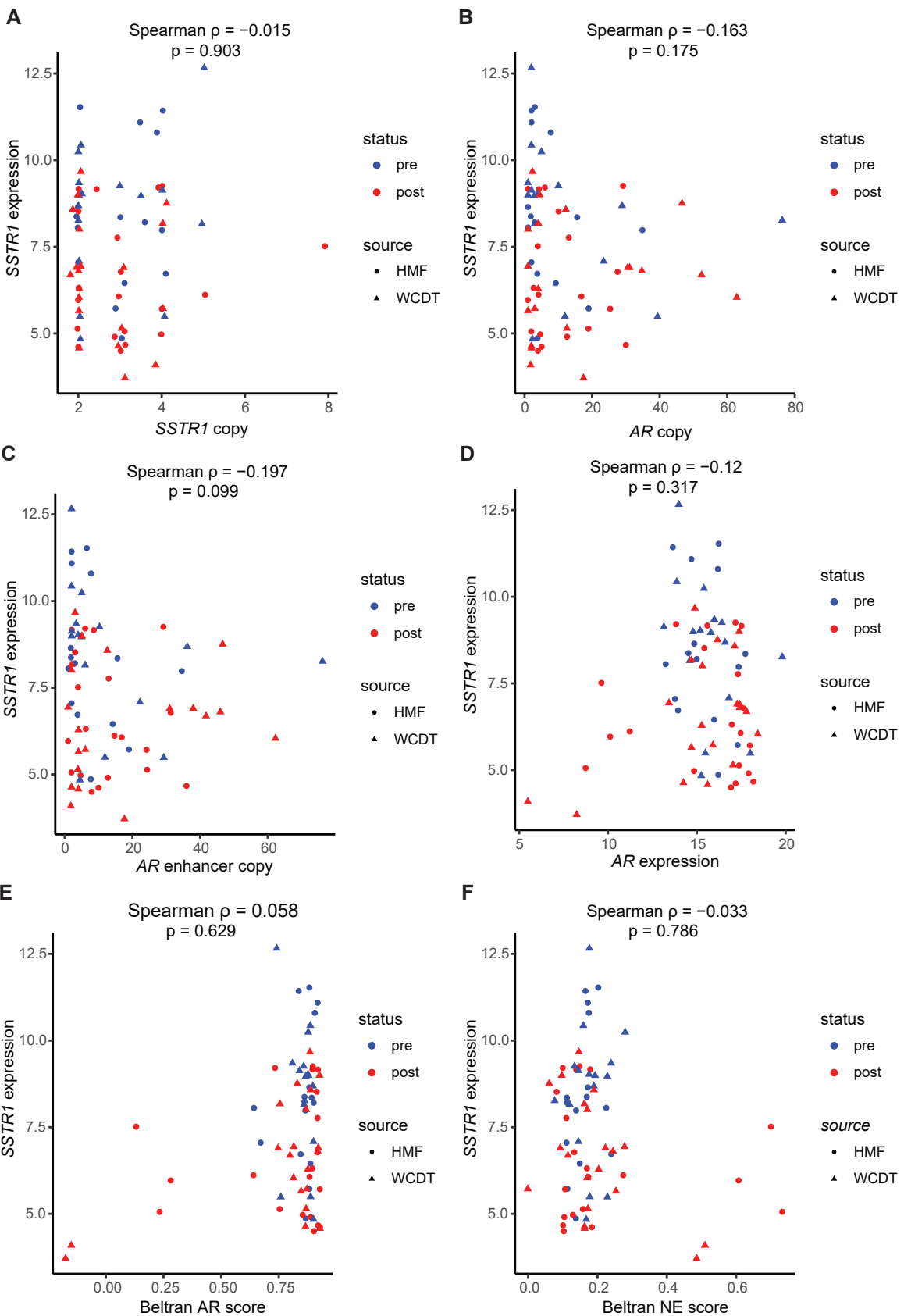
● Shallow Deletion

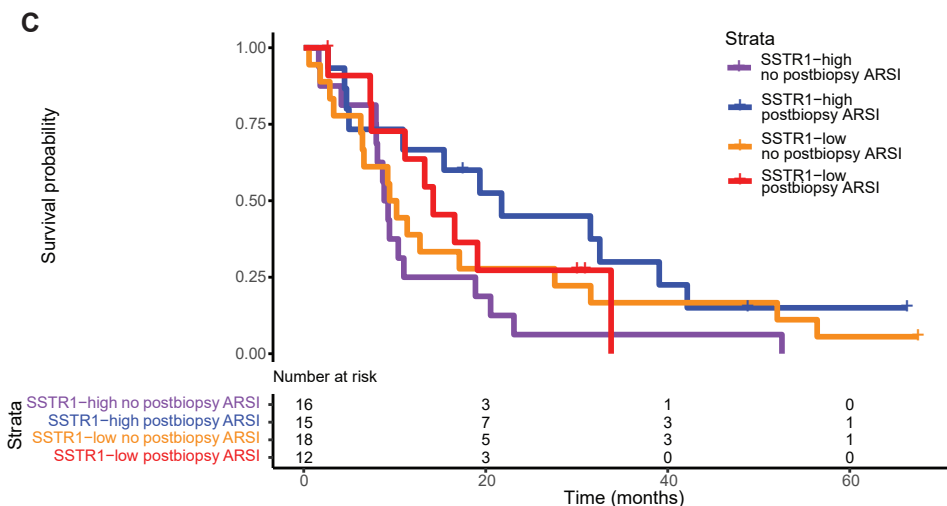
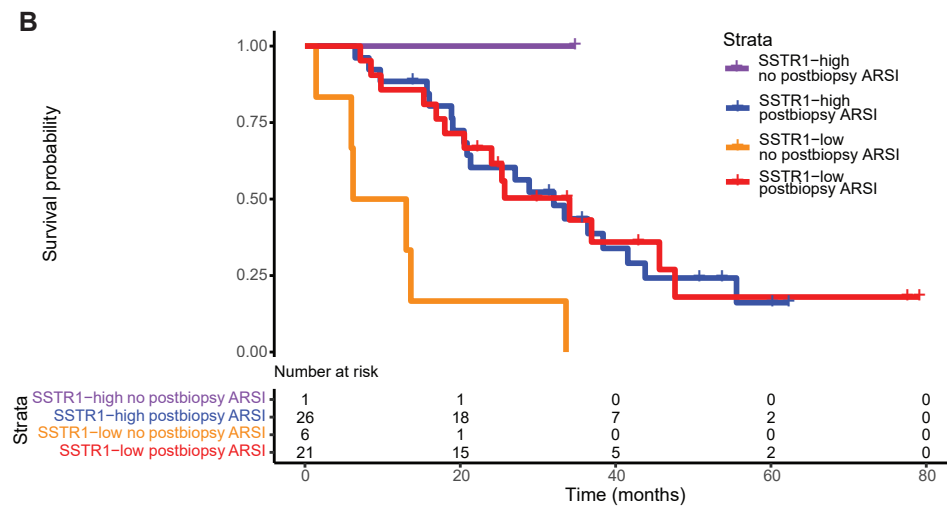
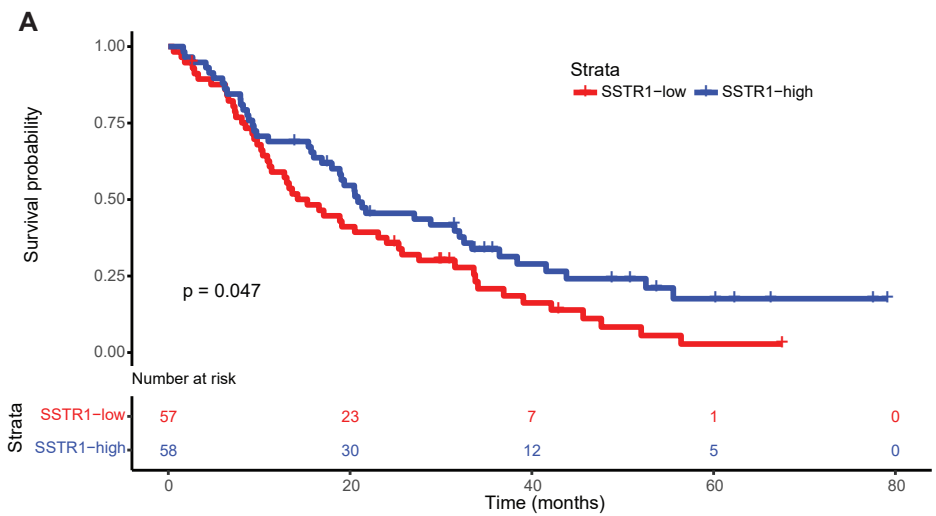
● Not mutated

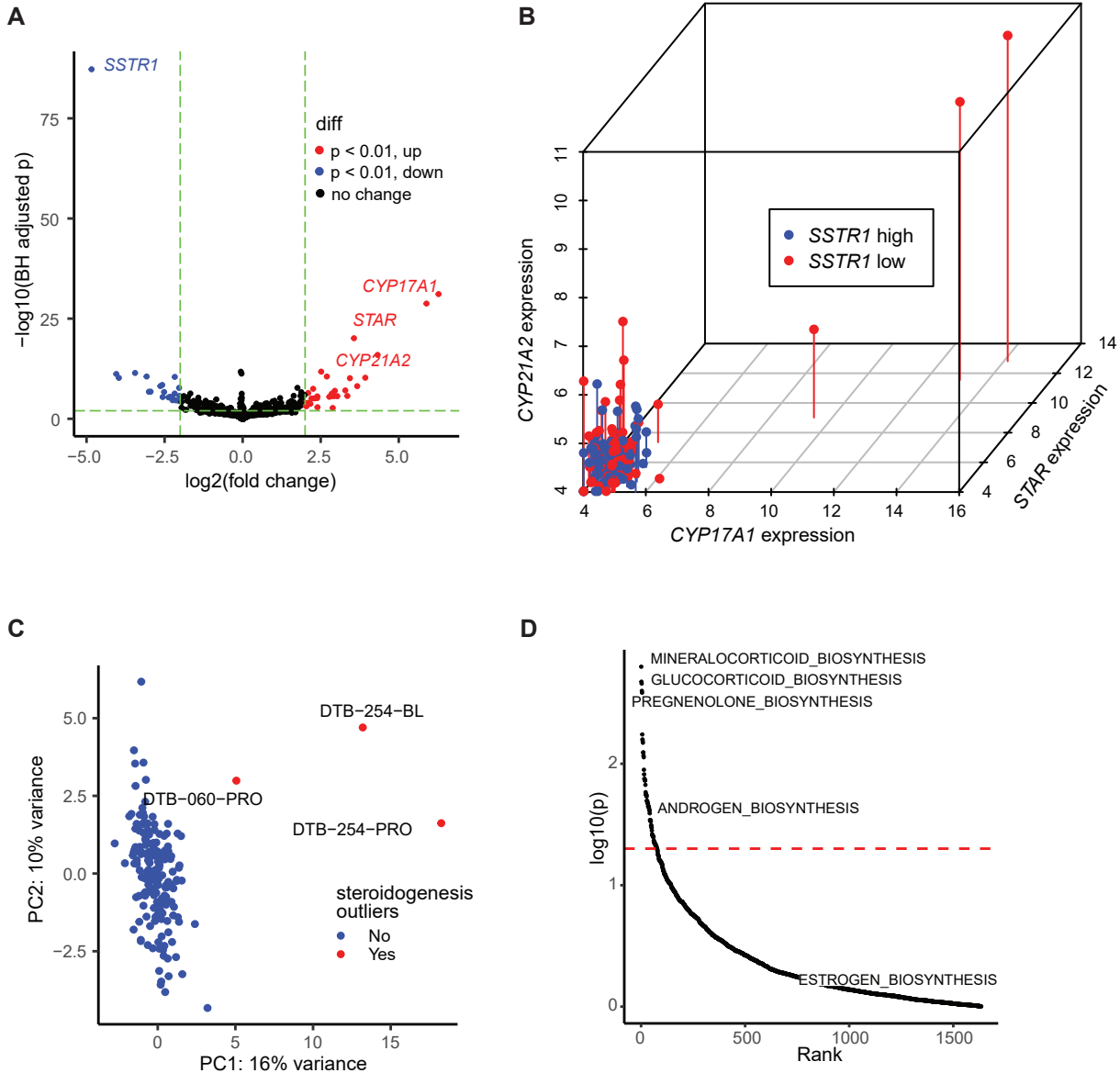
○ Gain

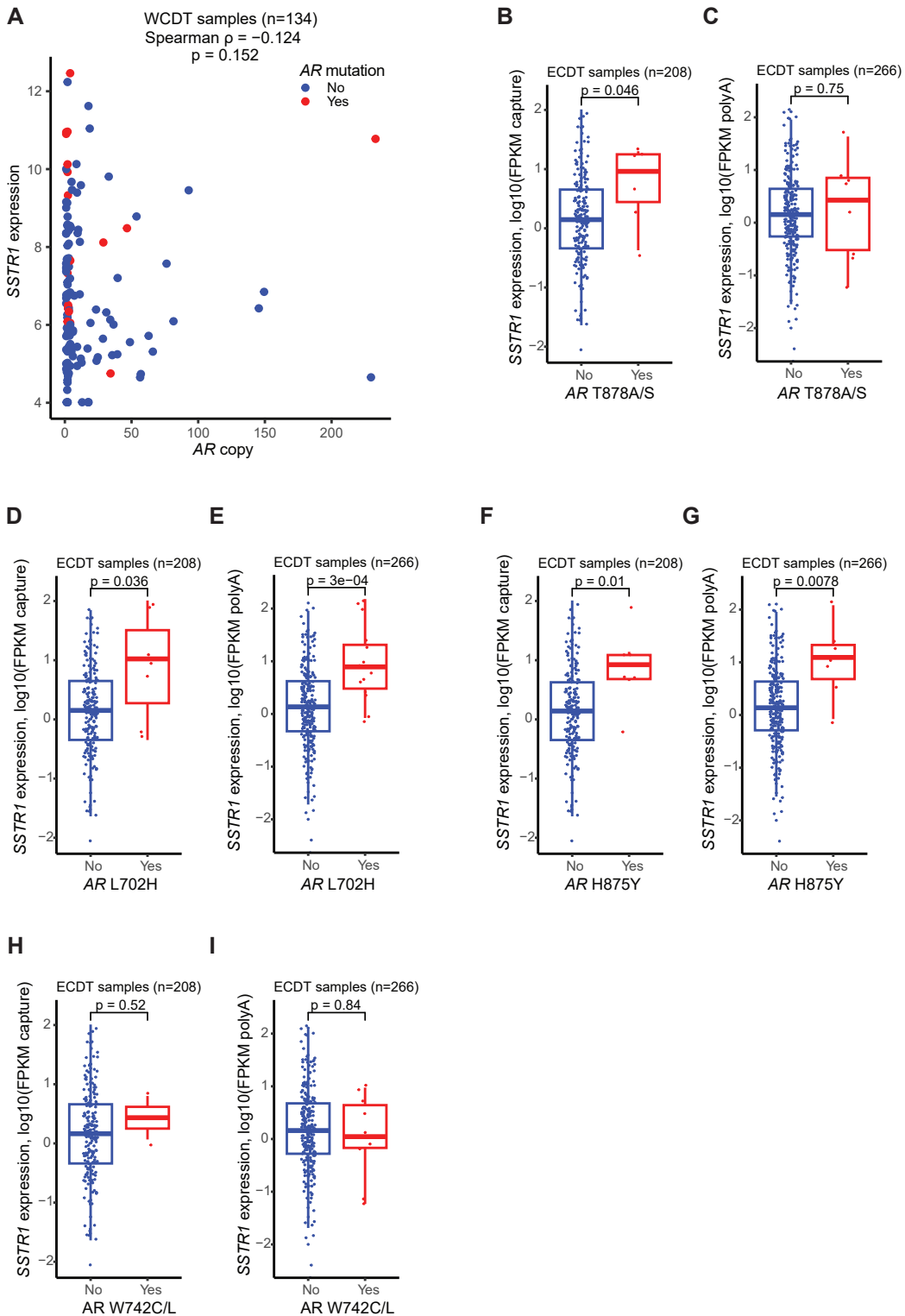
● Deep Deletion

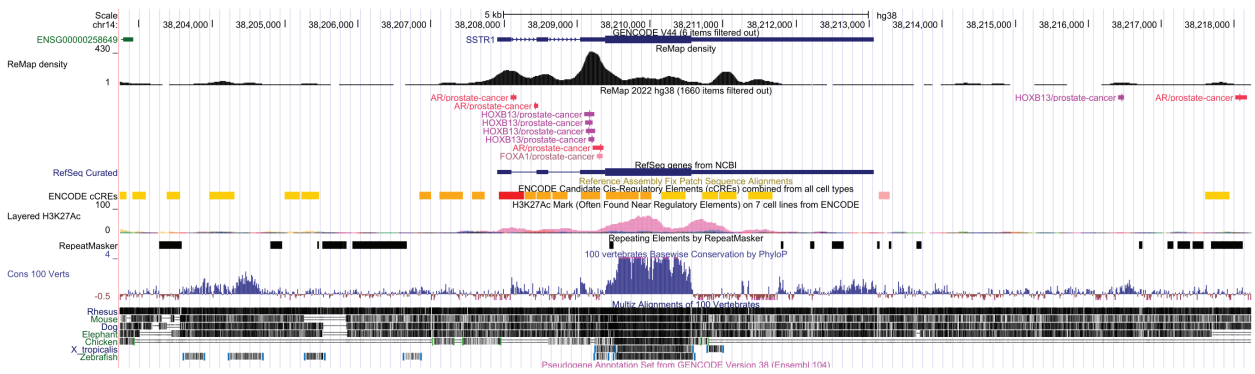


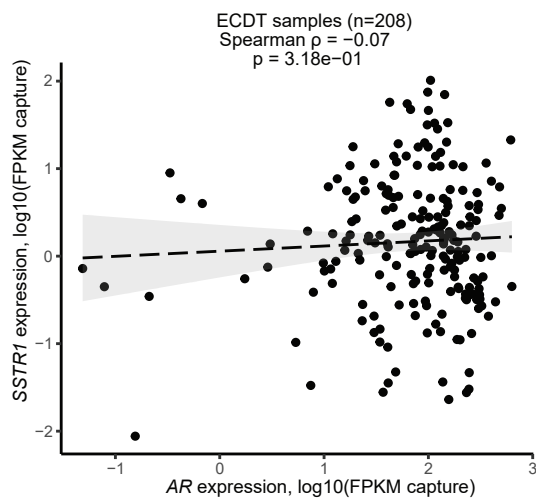
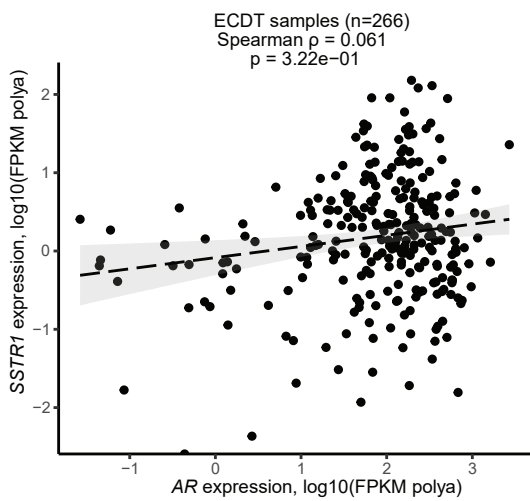
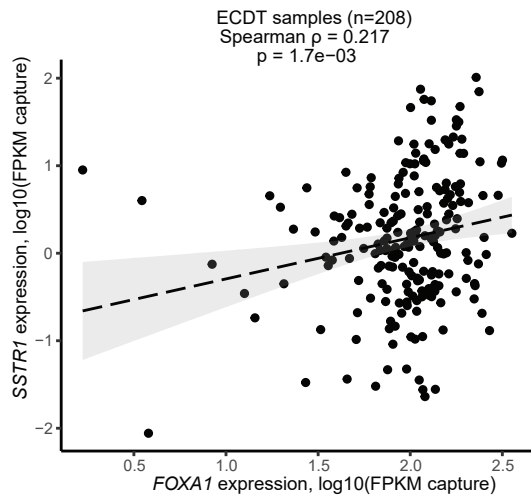
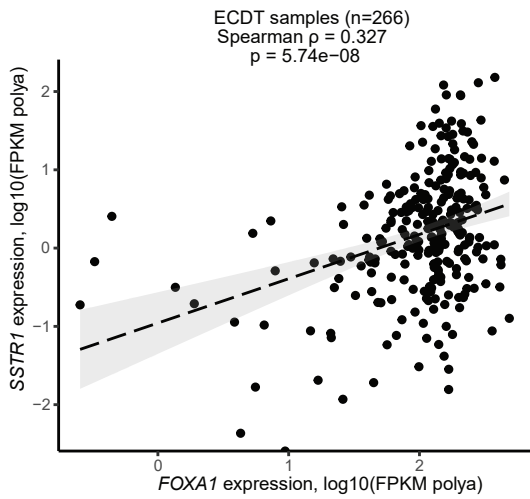
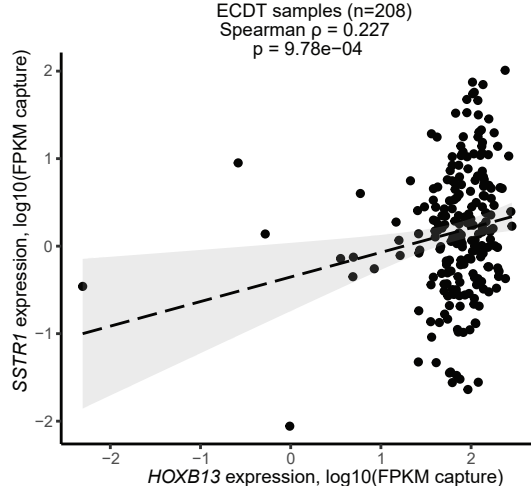
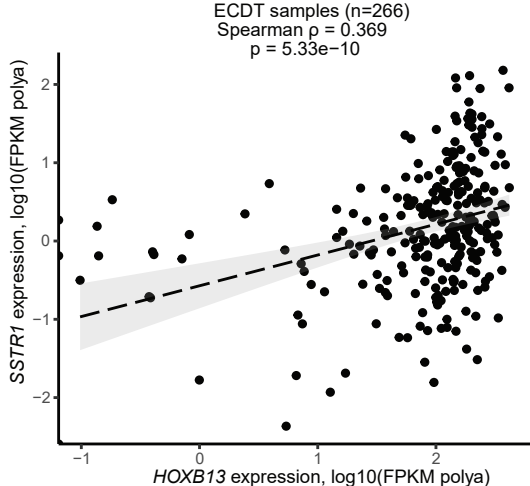


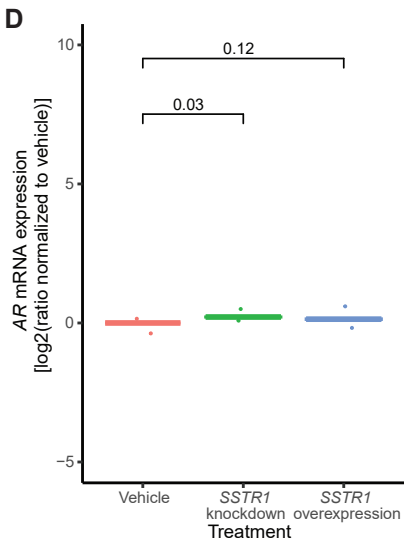
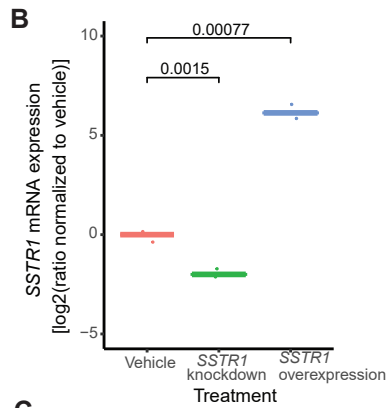
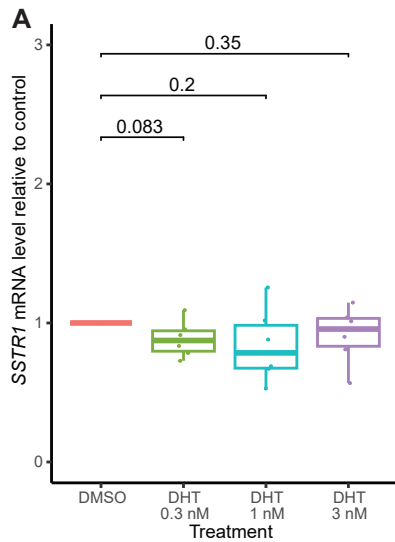




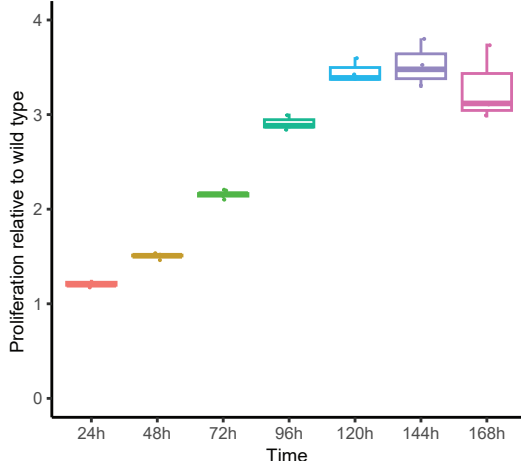




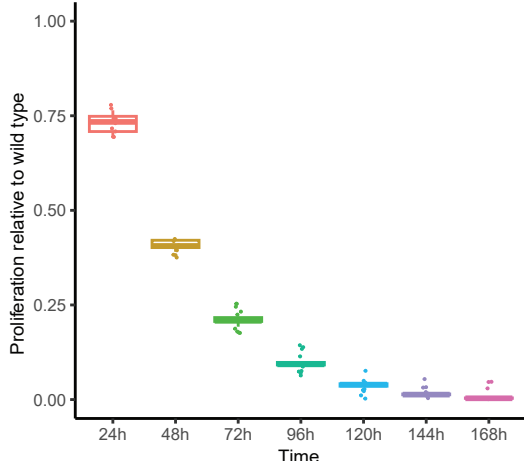
**A****B****C****D****E****F**



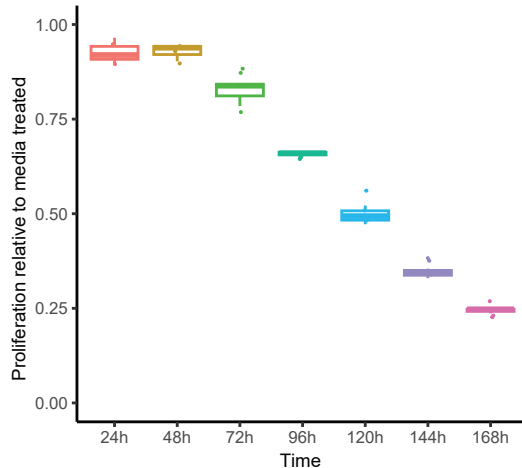
**E**  
22Rv1 cells, SSTR1 knockdown  
 $p$  (72h) =  $2.05e-04$ ;  $p$  (168h) =  $1.09e-02$



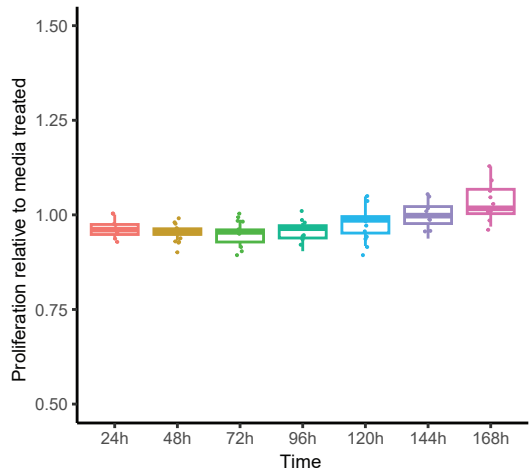
**F**  
22Rv1 cells, SSTR1 overexpression  
 $p$  (72h) =  $2.91e-17$ ;  $p$  (168h) =  $1.90e-25$



**G**  
22Rv1 cells, treated with Pasireotide 40 uM  
 $p$  (72h) =  $1.16e-02$ ;  $p$  (168h) =  $2.43e-05$



**H**  
22Rv1 cells, treated with Cyclosomatostatin 10 uM  
 $p$  (72h) =  $2.66e-04$ ;  $p$  (168h) =  $7.36e-02$



### **Supplemental Figure 1**

**Genomic landscape of the 45 paired mCRPC biopsies obtained before and after ARSI therapy.** Samples are split by pair (patient), and patients are sorted by the upstream *AR* enhancer (reported by Quigley et al., 2018) copy number of the resistant tumor post-ARSI.

### **Supplemental Figure 2**

**Patient-level summary of the 45 paired mCRPC biopsies stratified by sample source (WCDT vs HMF) and ARSI treatment status (pre vs post).** (A) Tumor purity. (B) Tumor ploidy. (C) Tumor mutation burden (TMB) per Mb. (D) Structural variant (SV) burden. **HMF:** Hartwig Medical Foundation. **WCDT:** West Coast Dream Team. P-values were calculated using two-sided paired Wilcoxon tests.

### **Supplemental Figure 3**

**For variants detected both pre-ARSI and post-ARSI in each patient, change in variant allele frequency (VAF) is highly correlated with change in estimated tumor purity.** Data represent all variants detected as such in the 45 paired mCRPC biopsies.

### **Supplemental Figure 4**

**Both *AR* and the upstream *AR* enhancer acquire further copy gains post-ARSI.** Figure panels show the copy number of *AR* (A) and the upstream *AR* enhancer (reported by Quigley et al., 2018, B), respectively, of the 45 paired mCRPC biopsies stratified by sample source (HMF vs WCDT).

### **Supplemental Figure 5**

***AR* mutations and *AR* gene/enhancer amplifications are not significantly associated with the duration of response to ARSI therapy (i.e., abiraterone or enzalutamide in the current study).** (A-C) *AR*-related genetic alterations detected post-ARSI. (D-F) *AR*-related genetic alterations detected pre-ARSI.

### **Supplemental Figure 6**

***AR* gene or enhancer-amplified mCRPC tumors without tandem duplications detected as the underlying events tend to have higher copy numbers, suggesting that extrachromosomal DNA may be a potential mechanism driving the amplifications.** (A) *AR* copy number is significantly higher in such tumors. (B) *AR* upstream enhancer copy number shows a similar trend.

### **Supplemental Figure 7**

**The fractions of AR-V7 or full-length AR (AR-FL) are not significantly different in mCRPC tumors before and after ARSI therapy, but some tumors show large numerical changes.** (A-B) AR-V7 and AR-FL fractions in 31 pre-ARSI and 40 post-ARSI samples. (C-D) AR-V7 and AR-FL fractions in 31 pairs.

### **Supplemental Figure 8**

**The androgen biosynthesis pathway activity assessed by RNA-seq is not significantly different in mCRPC tumors before and after ARSI therapy but shows a decreasing trend in the three tumors switching to an AR-independent phenotype as reflected by a high NE score (>0.4 as reported by Beltran et al., 2016).** (A-B) Androgen biosynthesis activity in all samples and the 31 pairs, respectively. (C-D) Androgen biosynthesis activity in the 28 pairs with post-ARSI Beltran NE score ≤0.4 and the 3 pairs >0.4, respectively.

**Supplemental Figure 9**

**Copy number of C4 is significantly increased post-ARSI.**

**Supplemental Figure 10**

**AR is not predicted to bind to C4.** A survey of cistromeDB nominates AR as the top transcription factor binding to C1-C3 based on the extent of overlaps with publicly available ChIP-seq datasets (**A-C**). In contrast, there is a lack of AR binding predicted in C4 (**D**).

**Supplemental Figure 11**

**FOXA1 but not steroid receptors are predicted to bind to C4.** Sets of assay for transposase-accessible chromatin with sequencing (ATAC-seq) peaks of human mCRPC (data from Tang et al., 2022) overlapping C1-C3 (**A**) and C4 (**B**) harbor distinct transcription factor (TF) binding motifs based on the Analysis of Motif Enrichment. While steroid receptors are predicted to bind to C1-C3, a distinct set of TFs are predicted to bind to C4, including FOXA1.

**Supplemental Figure 12**

**FOXA1 and AR are co-expressed in WCDT samples.**

**Supplemental Figure 13**

**FOXA1 ChIP-seq peaks are observed in C4 in multiple prostate cancer cell lines, primary prostate cancer, and mCRPC (data from ReMap2022).**

**Supplemental Figure 14**

**Removing the batch effect due to sample source (HMF versus WCDT) in RNA-seq analysis.** (**A**) Principal component analysis (PCA) before correcting the RNA-seq data for sample source. (**B**) PCA after correcting for sample source.

**Supplemental Figure 15**

**Variability of gene expression increases post-ARSI across all 22 genes used for the molecular subtyping of mCRPC by Labrecque et al., 2019.** Var(post) and Var(pre) denote the variance of gene expression in post-ARSI and pre-ARSI samples, respectively.

**Supplemental Figure 16**

**Measuring mCRPC transcriptional phenotypes using the subtyping scheme reported by Tang et al., 2022 (defined by transcription factor drivers) further highlights tumor heterogeneity associated with ARSI therapy.** (**A-D**) The four subtype scores (AR, WNT, NEPC, and SCL) in 31 pairs before and after ARSI therapy. No significant difference was observed, but some pairs showed dramatic changes after ARSI therapy. (**E**) The four subtype scores seem to measure different aspects of tumor transcriptional profiles, as reflected by a frequent lack of correlation between changes in these scores. (**F**) Principal component analysis using the changes in the four subtype scores highlights four post-ARSI outliers. (**G-L**) Pairwise scatter plots of the four subtype scores in 31 pairs with RNA-seq data. Pairs are labeled with directed linear segments (pre-ARSI → post-ARSI).

**Supplemental Figure 17**

**ChIP-seq signals of FOXA1 observed in the promoter of LMO3 in mCRPC are distinct from those in primary prostate cancer (ReMap2022; Hammal et al., 2022).** *LMO3* encodes a neuroendocrine transcription factor and is the most significantly upregulated gene in the unpaired RNA-seq analysis of mCRPC biopsies.

**Supplemental Figure 18**

**FGFR pathways are among the most upregulated post-ARSI in RNA-Seq analysis. (A)**

Volcano plot of unpaired RNA-seq analysis of Reactome pathways highlights increased activities of multiple FGFR pathways post-ARSI. **(B)** Component genes of the Reactome FGFR3 and FGFR2 pathways are shown in the Venn diagram.

**Supplemental Figure 19**

**SSTR1 is highly expressed in primary prostate cancer compared to other cancer types** (TCGA data, cancer types sorted by median SSTR1 mRNA).

**Supplemental Figure 20**

**SSTR1 is expressed in mCRPC cells rather than immune cells in the tumor** (data from He et al., 2021 and visualized using the Single Cell Portal).

**Supplemental Figure 21**

**SSTR1 expression in mCRPC biopsies.** SSTR1 expression is not associated with SSTR1 copy number **(A)**, AR copy number **(B)**, the upstream AR enhancer copy number **(C)**, AR mRNA level **(D)**, Beltran AR score **(E)**, or Beltran neuroendocrine (NE) score **(F)**.

**Supplemental Figure 22**

**Tumor SSTR1 mRNA as related to survival in a retrospective analysis of mCRPC patients.** **(A)** Higher SSTR1 expression is associated with better overall survival in WCDT samples. **(B and C)** Survival curves stratified by SSTR1 expression status (high versus low) and post-biopsy ARSI exposure (yes versus no) in patients with ARSI-naïve and ARSI-exposed mCRPC tumors, respectively, in WCDT.

**Supplemental Figure 23**

**Excessive steroidogenesis is associated with ARSI resistance in a subset of SSTR1-low mCRPC.** **(A)** Differential gene expression analysis contrasting SSTR1-high versus SSTR1-low tumors highlights upregulation of steroidogenesis genes including CYP17A1, STAR, and CYP21A2, in SSTR1-low mCRPC, driven by three outlier samples **(B)**. **(C)** Principal component analysis using expression data of 24 genes in the five steroidogenesis pathways (mineralocorticoid, glucocorticoid, androgen, estrogen, and pregnenolone) confirms that the three SSTR1-low tumors are indeed outliers in steroidogenesis activity. **(D)** These three tumors maintain a more pronounced activity of mineralocorticoid, glucocorticoid, and pregnenolone biosynthesis rather than androgen biosynthesis compared to the other tumors.

**Supplemental Figure 24**

**SSTR1 mRNA as related to AR mutations.** **(A)** SSTR1 expression is not associated with AR copy number in 134 WCDT samples with both WGS and RNA-seq data available. **(B-I)** In ECDT, the presence of an AR hotspot mutation such as T878A/S, L702H, and H875Y, but not W742C/L, is associated with increased SSTR1 expression. FPKM: Fragments Per Kilobase of transcript per Million mapped reads.

**Supplemental Figure 25**

**ChIP-seq signals of AR, FOXA1, and HOXB13 are observed in mCRPC patient-derived xenografts (PDXs) overlapping with exon 3 of SSTR1 (ReMap2022; Hammal et al., 2022).**

**Supplemental Figure 26**

**FOXA1 and HOXB13, but not AR, are co-expressed with SSTR1 in ECDT samples.**

Analyses are stratified by RNA-seq method (“capture” vs “polyA”). FPKM: Fragments Per Kilobase of transcript per Million mapped reads.

**Supplemental Figure 27**

**SSTR1 is anti-proliferative in mCRPC and amenable to pharmacological intervention. (A)**

SSTR1 mRNA level, as assessed by reverse transcription-quantitative polymerase chain reaction (RT-qPCR), did not change after 48 hours of dihydrotestosterone (DHT) treatment in 22Rv1 cells.

**(B and C)** RT-qPCR and western blot validation, respectively, of SSTR1 stable knockdown assay using Clustered Regularly Interspaced Palindromic Repeats interference (CRISPRi) and SSTR1 stable overexpression assay in 22Rv1 cells. All bands indicate ~80kDa as validated by the vendor (Cell Signaling Technology). The lanes were run on the same gel but were noncontiguous.

**(D)** AR mRNA expression, as assessed by RT-qPCR, did not seem to change significantly with SSTR1 knockdown or overexpression in 22Rv1 cells.

**(E)** SSTR1 knockdown significantly increased the proliferation of 22Rv1 cells using the IncuCyte cell count proliferation assay, and SSTR1 overexpression had the opposite effect **(F)**.

**(G)** Pasireotide, the only FDA-approved drug with SSTR1 agonist activity, significantly inhibited the proliferation of 22Rv1 cells, whereas the SSTR1 antagonist cyclosomatostatin did not seem to have a substantive effect **(H)**.

P-values were calculated using Student's t-test.